

DESIGN OF QUASI-TERMINATOR ORBITS NEAR PRIMITIVE BODIES

Gregory Lantoine, Stephen B. Broschart, and Daniel J. Grebow *

Quasi-terminator orbits are a class of quasi-periodic orbits around a primitive body that exist in the vicinity of the well-known terminator orbits. The inherent stability of quasi-terminator trajectories and their wide variety of viewing geometries make them a very compelling option for primitive body mapping missions. In this paper, we discuss orbit design methodologies for selection of an appropriate quasi-terminator orbit that would meet the needs of a specific mission. Convergence of these orbits in an eccentric, higher-fidelity model is also discussed with an example case at Bennu, the target of the upcoming NASA's OSIRIS-REx mission.

INTRODUCTION

A lot of missions aimed at the characterization of small primitive bodies (i.e., comets, asteroids, and small planetary moons) are currently in flight and under development. Prominent examples are ESA's Rosetta and MarcoPolo-R, JAXA's Hayabusa-2, and NASA's OSIRIS-REx. These primitive body missions must typically include some sort of global mapping campaign where visible spectrum imaging is used to build up image collections and global shape models. For these applications, it is necessary to collect data from directions that encompass the whole body. In particular, for good global imaging and shape model we need images of the complete lit side of the object from a variety of angles and orientations.

The standard technique to perform mapping is to rely on station keeping, such as controlled polar orbits or vertical hovering (where the spacecraft stays along the line joining the Sun and the body through frequent instantaneous maneuvers) [1]. For example, OSIRIS-REx is expected to quasi-hover around 1999 RQ36 for one month [2]. Likewise, MarcoPolo-R should perform station keeping for one month to stay on a far station location close to the Sun-asteroid line [3]. However, these strategies require maneuvers to maintain the spacecraft on a suitable orbit, which therefore introduces additional constraints, such as intensive operator interventions, limited mission lifetime, and reduced accuracy of the estimate of the asteroid physical parameters.

It is therefore crucial to look for stable solutions that would provide extensive coverage without the need of controlling the spacecraft. Finding such desirable stable orbits is a challenge because the dynamical environment near small bodies is highly perturbed by solar pressure and gravitational

*Mission Design Engineers, Mission Design and Navigation Section, Jet Propulsion Laboratory, California Institute of Technology, M/S: 301-121, 4800 Oak Grove Dr., Pasadena, CA 91109.

©2013 California Institute of Technology. Government sponsorship acknowledged.

forces from the asteroid and the Sun. Even the well-known stable retrograde equatorial orbits cannot exist in this environment [4]. The design methodology of mapping orbits therefore requires a paradigm shift by taking advantage of the highly nonlinear dynamics near a primitive body instead of minimizing their effects.

Recently, a new class of stable, quasi-periodic orbits has been discovered in the solar pressure perturbed Hill model around a primitive body [5, 6]. These trajectories are called ‘quasi-terminator’ orbits because they are part of quasi-periodic tori around the well-known periodic terminator orbits that exist in that environment. Many of these quasi-periodic orbits offer a range of sun-lighted surface viewing geometries while presenting long-term stability and robustness characteristics. Contrary to quasi-hovering strategies, these orbits are therefore ballistic and do not nominally require active control.

This paper therefore describes a design methodology for generating quasi-terminator orbits that could support mapping campaigns of primitive bodies. First, the paper develops the background necessary to explain what a quasi-terminator orbit is and how it works. Then, the design space is explored and useful plots are provided to enable mission analysts to quickly select an appropriate quasi-terminator orbit that would meet the mapping campaign needs of a specific mission. Finally, a continuation approach, relying on a multiple shooting differential correction algorithm, is used to transition ideal quasi-terminator orbits to a higher-fidelity dynamical model. The converged solutions are shown to retain good design characteristics. Throughout the paper, we will illustrate the techniques developed on a case study at asteroid 1999 RQ36 (recently renamed Benu), the target of the upcoming NASA’s OSIRIS-REx mission.

BACKGROUND

Equations of Motion

The dynamics of a spacecraft in close proximity to most primitive bodies are primarily driven by the solar radiation pressure and the gravitational attraction of the Sun and primitive body (i.e., the primaries). Let $\mathbf{r} = [x, y, z]$ and $\mathbf{v} = [\dot{x}, \dot{y}, \dot{z}]$ represent the normalized spacecraft position and velocity vectors, respectively, and their coordinates with respect to a rotating frame centered on the primitive body. This frame is defined such that the \hat{x} direction points from the Sun to the primitive body, the \hat{z} direction is aligned with the angular velocity of the primaries, and the \hat{y} direction completes the right-handed triad. Then the Augmented Normalized Hill Three-Body Problem (ANH3BP) describes the spacecraft motion near a point-mass primitive body under the influence of SRP and solar tide in this coordinate frame (assuming the primitive body is on an heliocentric circular orbit). The equations of motion (adapted from [7]) can be written:

$$\begin{aligned}\ddot{x} &= 2\dot{y} + 3x - x/|\mathbf{r}|^3 + \beta \\ \ddot{y} &= -2\dot{x} - y/|\mathbf{r}|^3 \\ \ddot{z} &= -z - z/|\mathbf{r}|^3,\end{aligned}\tag{1}$$

Only one parameter, β , appears in these equations. This parameter is the nondimensional acceleration due to SRP (assuming a spherical spacecraft) and is computed using Eq. 2:

$$\beta = \left(\frac{G_1}{(m/A)R^2} \right) \left(\frac{1}{N} \right)^2 \left(\left(\frac{\mu_{pb}}{\mu_{Sun}} \right)^{1/3} R \right)^{-1} = \frac{G_1}{(m/A)\mu_{Sun}^{2/3}\mu_{pb}^{1/3}},\tag{2}$$

where G_1 is the solar flux constant ($\approx 1 \times 10^{14}$ (kg km)/s²), (m/A) is the effective mass-to-projected area ratio for the spacecraft, R is the constant distance between the Sun and the primitive body, $N = \sqrt{\mu_{Sun}/R^3}$ is the mean motion of the primary orbits, μ_{pb} is the gravitational parameter of the primitive body, and μ_{Sun} is the gravitational parameter of the Sun (1.327×10^{11} km³/s²). Moreover, the ANH3BP is time invariant and admits an integral of the motion, the well-known Jacobi constant:

$$C = \frac{1}{2} \|\mathbf{v}\|^2 - 1/\|\mathbf{r}\| - \frac{3}{2}x^2 + \frac{1}{2}z^2 - \beta x, \quad (3)$$

Note that for the normalization, the unit length is $(\mu_{pb}/\mu_{Sun})^{1/3}R$ and the unit time is $1/N$.

Terminator orbits

Terminator orbits are a well-known class of orbits that exhibits stable behavior when solar radiation pressure is a significant contributor to the orbit dynamics [8, 7, 9, 10, 4, 11, 12, 13]. The terminator orbits are oriented such that the asteroid-sun line is perpendicular to the orbit plane. The orbit center is also slightly offset away from the Sun from the primitive body center. As β increases from zero, the terminator orbits move from being highly eccentric (as in the circular-restricted three-body problem (CR3BP) [14]) to nearly circular [8].

Unfortunately, the terminator orbit geometry only allows for poor visibility of the lit side of the object. Terminator orbits are therefore undesirable for shape modeling and surface properties mapping.

Quasi-Terminator orbits (QTOs) and Resonant Terminator orbits (RTOs)

Quasi-terminator orbits are a class of quasi-periodic orbits about small bodies that offers a much wider range of Sun-relative geometries [5, 6]. These orbits originate from the two center manifolds around the periodic terminator orbits, and evolve on an invariant torus described by two frequencies. In fact, it has been demonstrated that the monodromy matrix of the terminator orbits have two pairs of unit-magnitude, complex conjugate eigenvalues, which in a linear sense implies the existence of nearby quasi-periodic motion [15, 16, 17].

Quasi-terminator orbits do not exclusively lie in the terminator plane, and their geometry can allow for low nadir pointing phase angle, with various ranges from the illuminated surface. In addition, these orbits are stable and do not nominally require any station-keeping maneuvers. Thus, quasi-terminator orbits are attractive for global mapping campaigns at primitive bodies.

The trajectories on the two sets of invariant tori are geometrically distinct. The *Sun-side quasi-terminator orbits* extend away from the terminator plane toward the sunlit side. These orbits are therefore attractive for global mapping campaigns at primitive bodies. On the other hand, the *dark-side quasi-terminator orbits* extend away from the terminator plane toward the shadowed-side of the primitive body. These orbits have close encounters over the lit side, so they are favorable in a reconnaissance phase to select a potential landing or sampling site. Other applications could also involve inferring the gravity field, internal structure and composition of the body through global radar measurements.

A special class of quasi-terminator orbits is also particularly interesting for mission design: the so-called *resonant terminator orbits* (RTOs) are special resonant, periodic cases of quasi-periodic motion, where the two frequencies of motion on the invariant torus are commensurate. Geometrically, an $m:n$ RTO makes m revolutions around the body before closing on itself, and m/n is the

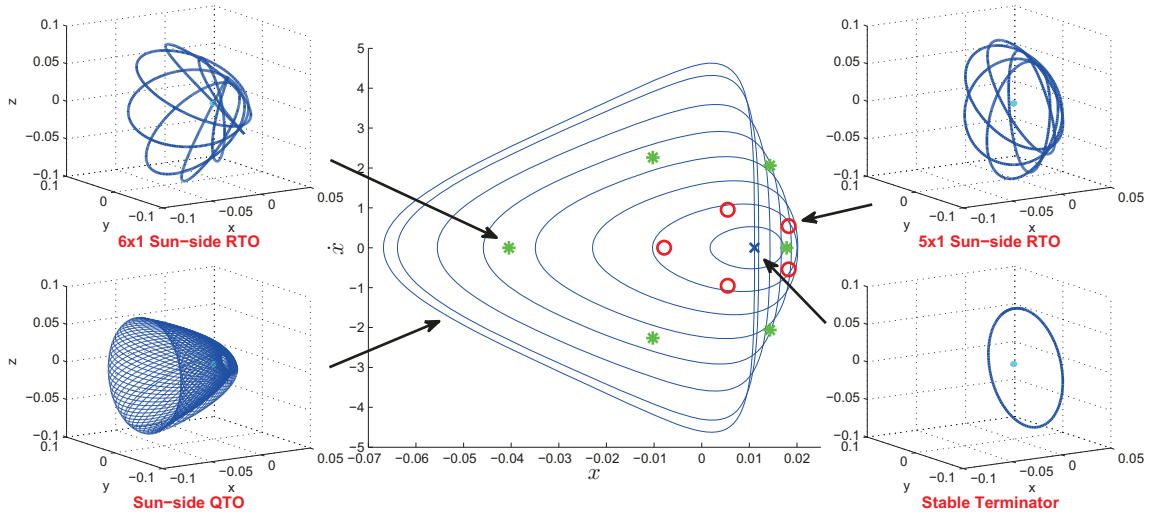


Figure 1: Poincaré section ($y = 0, \dot{y} > 0$) of Sun-side QTOs for $\beta = 25$ and $C = -6.8$. The spatial plots and Poincaré crossings for several RTOs are also shown. The last computed Sun-side torus of the family is also plotted in spatial coordinates.

frequency ratio of the RTO. In this paper, the characteristics of quasi-terminator orbits will be approximated by those of nearby RTOs since: 1) they are faster to compute than QTOs across a broad design space because they are found by simply following period-multiplying bifurcations with the terminator orbit family [12]; and 2) they are easier to characterize since they are periodic. Since RTOs are regularly embedded in the quasi-terminator orbits, we believe that no significant information is lost with that strategy.

For conciseness, we will focus only on the design of Sun-side RTOs for mapping campaigns. Typical examples of Sun-side families of QTOs and RTOs near the terminator orbits are shown in Figures 1 using a Poincaré section at $z = 0$ when $\dot{z} < 0$ with a fixed Jacobi constant C . The blue curves in these plots represent the 1-D intersection of the 2-D invariant torus of the QTOs with the Poincaré section. Motion that begins on one blue curve (i.e., on a particular torus) has all its subsequent intersections with the Poincaré section on that same curve. Each plot shows a variety of quasi-terminator and RTO solutions at the chosen energy level ($C = -6.8$), as well as nearby stable/unstable manifold structures.

CHOOSING A QUASI-TERMINATOR ORBIT

Previous work [6, 5] describes the characteristics of quasi-terminator orbits/RTOs and how to find them. This section focuses on how to choose a QTO/RTO for a global mapping scenario, presents charts to simplify the process of finding an initial state, and presents an example mapping orbit case consistent with the OSIRIS-REx mission.

Parameterization of Quasi-terminator Orbits

Since the normalized equations of motion (Eqs. 1) have only a single parameter β , the complete configuration space is 7-dimensional. Specifically, there are 6 Cartesian states (\mathcal{R}^6) and one positive real parameter β . In the region of stable quasi-periodic motion that exists near the terminator

and quasi-terminator orbit solutions, this space is filled with 3-frequency invariant tori. This paper is concerned with "quasi-terminator" motion, which evolves on a 2-frequency invariant torus [6, 5], and RTOs, which are a degenerate case of quasi-terminator motion where the two phase angles describing the location on the torus (v_1 and v_2) are not independent. Table 1 presents the dimensionality of various orbit spaces of interest, as well as sample parameterizations of the space.

Table 1: Dimensionality of Orbit Solution Spaces

	# of independent parameters	Example parameterization
Configuration space	7	$x, y, z, \dot{x}, \dot{y}, \dot{z}, \beta$
Stable region	7	$C, f_1, f_2, v_1, v_2, v_3, \beta$
Terminator orbits	3	C, v, β
Resonant terminator orbits	4	C, f, v, β
Sun-/Dark-side quasi-terminator orbits	5	C, f, v_1, v_2, β

Selecting a Quasi-terminator Orbit

For a fixed value of β , the remaining independent parameters that describe states on a quasi-terminator orbit consist of two geometric parameters defining the 2-D torus shape and two phase parameters that define the location on that torus. This understanding is useful when selecting a quasi-terminator orbit. Most importantly, it can be understood that two geometry parameters can be selected independently, but any other geometric properties of the orbits will be determined by those choices. For example, a designer choosing a global mapping orbit could specify the periapsis radius and the minimum Sun-body-S/C angle achieved by an orbit, but the maximum orbit radius would be determined by those choices. Any two geometry parameters could be specified, so in another example the designer may choose an orbit period and a torus frequency ratio for an RTO and the minimum ϕ and radius would be determined by those choices. The two phase parameters can be specified in a number of ways. One way is to specify Cartesian coordinates directly (so long as they are on the corresponding 2-D torus). An example used here is to specify $y = 0$ and $\dot{x} = 0$.

In [6, 5], we presented plots of various geometric characteristics of quasi-terminator orbits as a function of β , as well as unit length and time parameters for some realistic mission scenarios. Speaking roughly, it can be concluded from that data that quasi-terminator orbits are best for mapping applications for β values between 10 and 200. Figures 2 and 3 show the properties of quasi-terminator orbits at β values in this range in detail. These plots can be used to assess the rough geometric characteristics of a particular quasi-terminator orbit design. We've assumed $y = 0$ and $\dot{x} = 0$ here to set the phase angles, leaving a 3-D solution space. For β values between these 2-D slices shown, interpolation should yield a reasonable approximation of the orbit properties.

Getting initial conditions

Ideally, initial conditions from QTOs are derived from a database of numerically-generated periodic orbits and tori following the methods previously presented [6, 5]. However, for initial analysis and consideration of these orbits, creating such a database may require a prohibitive investment of

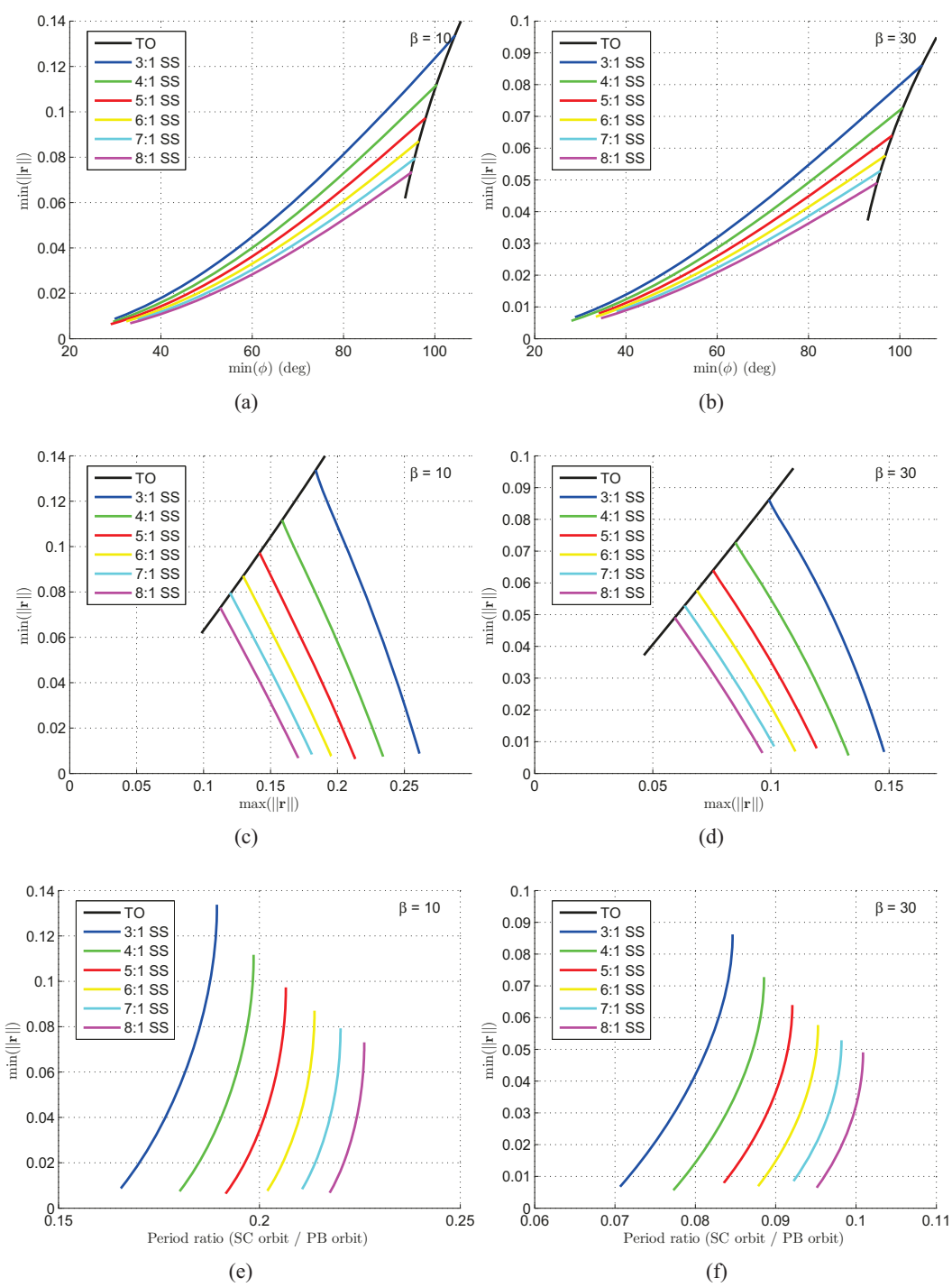


Figure 2: Important QTO/RTO properties for mapping orbit design at $\beta = 10, 30$.

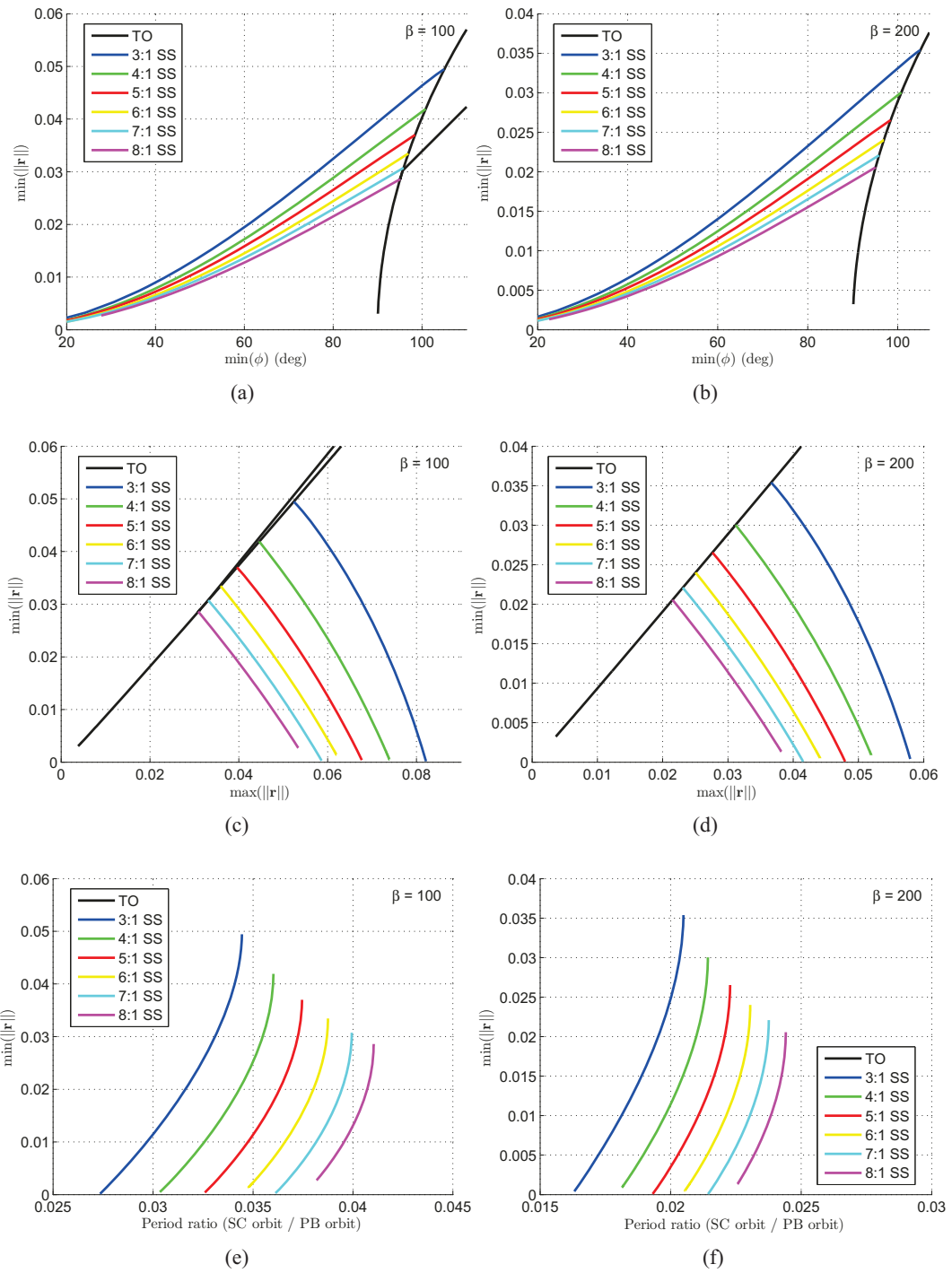


Figure 3: Important QTO/RTO properties for mapping orbit design at $\beta = 100, 200$.

effort. An alternative approach is to read normalized Cartesian coordinates off of a figure. Similar to above, the space of solutions is reduced to 3-D by fixing the phase angles for the state. Figures 4 and 5 proceed in a similar manner to the previous figures, presenting slices of the 3-D solution space. Here, the Cartesian initial state parameters are plotted as function of the geometric parameters of minimum orbit radius, minimum ϕ , and torus frequency ratio f (where the last two parameters are dependent). Approximate initial states from this plot can be dimensionalized using the appropriate length and time scales and propagated. Given the stability of these orbits, the propagated trajectory, which is most likely on a nearby 3-D torus, is probably good enough for most analysis purposes. The coordinates can also be tweaked iteratively toward the desired properties.

Example for OSIRIS-REx mapping orbit design

Table 2: Physical characteristics of Bennu

μ_{pb}	$4.057184e - 009 \text{ km}^3/\text{s}^2$
J_2	0.0127017
r_{pb}	250 m
R	1.126 AU
e	0.2

Throughout this paper, an example is presented for design of a quasi-terminator mapping orbit for the OSIRIS-REx spacecraft at the asteroid Bennu. Table 2 gives the main physical characteristics of Bennu and its orbit. The OSIRIS-REx spacecraft at Bennu has a β of about 30, given its estimated encounter mass of 1347 kg, a projected surface area of 14 m², and an average total reflectivity of 0.2 [18]. For this mapping orbit example, the following characteristics are desired.

- Achieves full range of geometry in 2 months or less
- Periapsis radius greater than 0.6 km
- Apoapsis radius at roughly 5 km
- Minimum Sun-body-S/C angle less than 50 deg

Figure 2 shows the characteristics of various RTOs at $\beta = 30$. Since only two geometric parameters can be specified explicitly, it is possible that all of the desired orbit characteristics cannot be met, and quasi-terminator orbits may not be the right choice. For the OSIRIS-REx example however, the desired mapping orbit characteristics can be met by an RTO with f between 5 and 7.

The following analysis will utilize an 6:1 Sun-side RTO with a minimum ϕ of 45 deg and a period of about two months. Figure 6(a) shows a spatial plot of this periodic orbit and Figure 6(b) indicates the quality of the mapping orbit by showing the groundtrack and altitude of the orbit relative to the Sun direction. These plots assume the dynamics of the ANH3BP, which have several key limitations to be discussed in the next section.

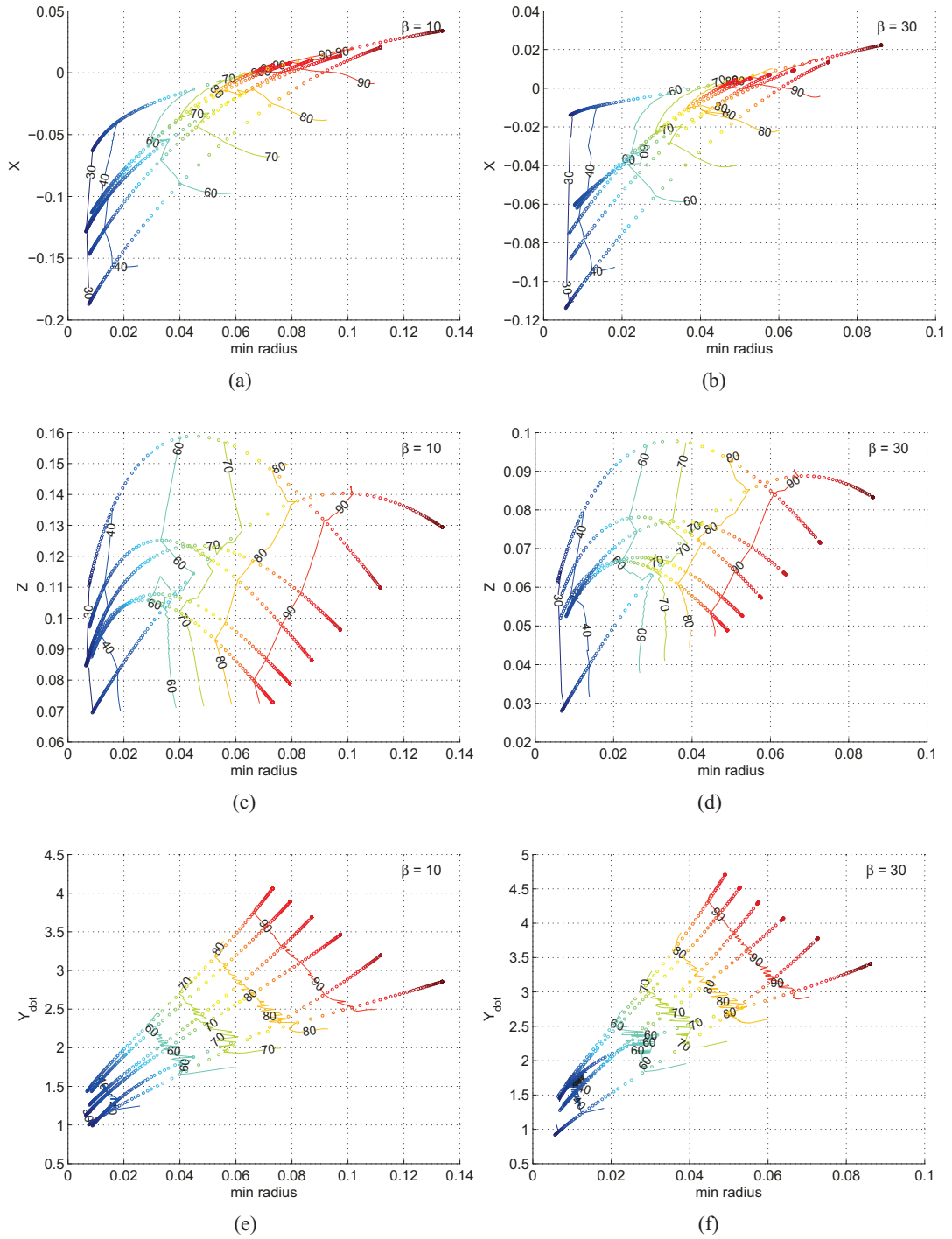


Figure 4: Initial state coordinates for mapping orbit design at $\beta = 10, 30$. Contours show minimum ϕ and f . y, x_{dot} , and z_{dot} are identically zero for RTOs.

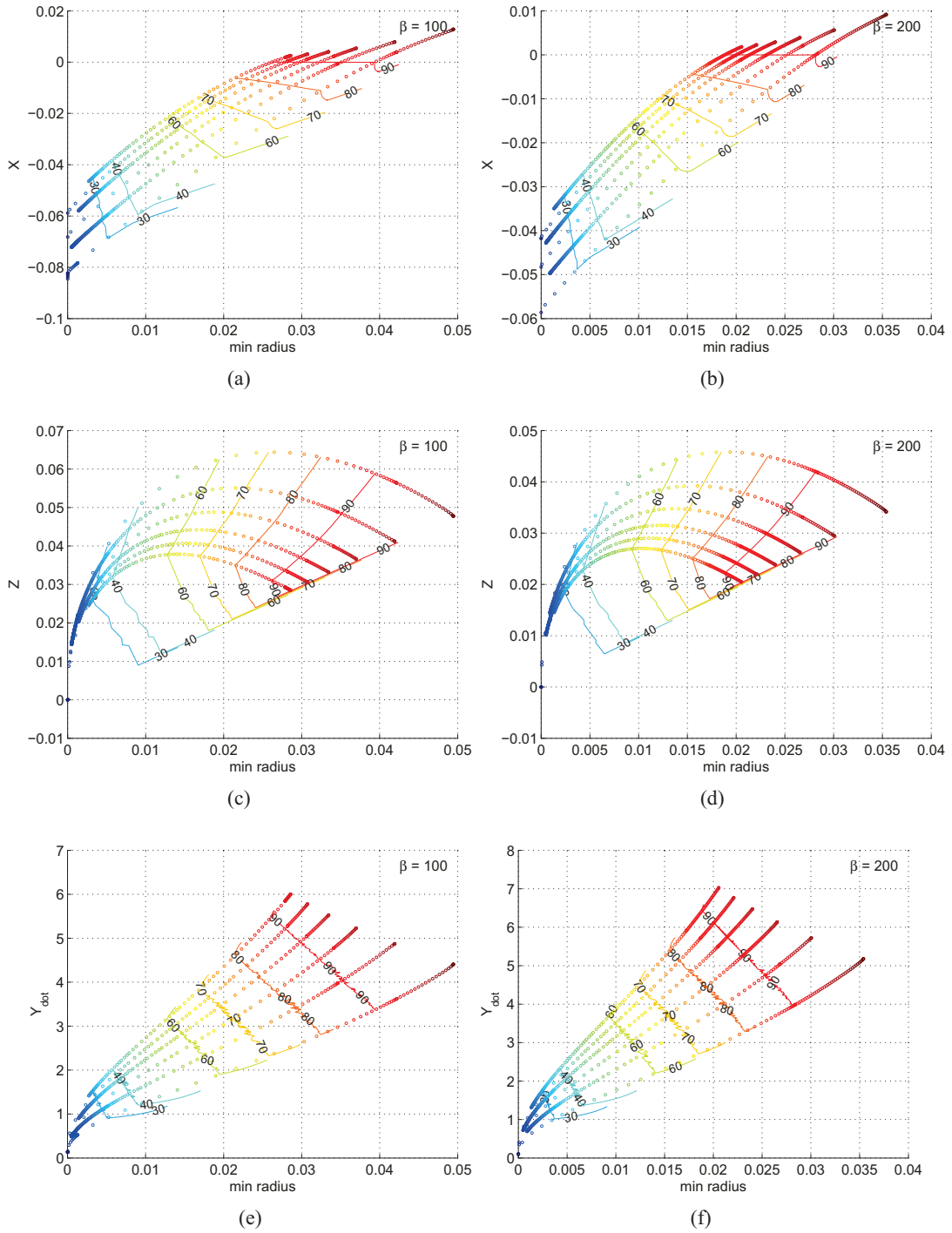


Figure 5: Initial state coordinates for mapping orbit design at $\beta = 100, 200$. Contours show minimum ϕ and f . y, x_{dot} , and z_{dot} are identically zero for RTOs.

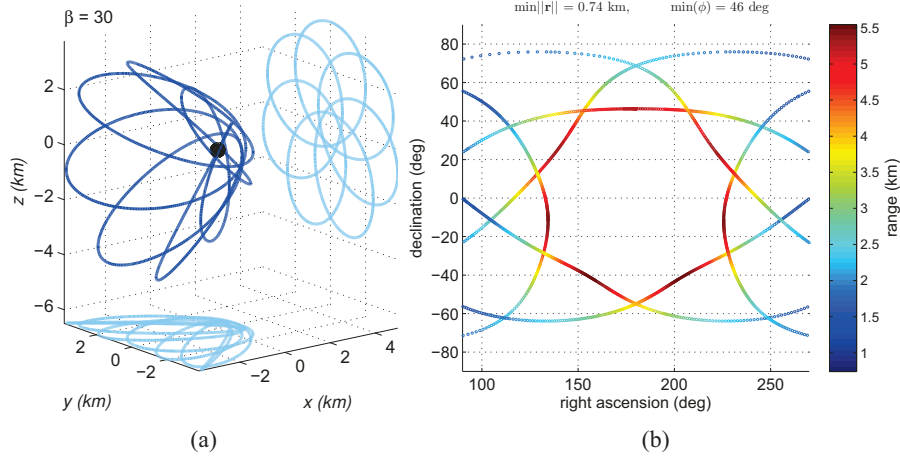


Figure 6: 6:1 RTO example mapping orbit in the ANH3BP consistent with the upcoming OSIRIS-REx mission parameters. (a) Spatial plot. (b) Groundtrack and altitude relative to the Sun.

TRANSITION TO HIGHER-FIDELITY MODEL

In the previous section, RTO families have been shown to offer a desirable variety of viewing geometry for primitive body missions while exhibiting linear stability in the ANH3BP. However, the real dynamical environment near a small body generally deviates significantly from the ideal ANH3BP model due to the eccentricity of body’s heliocentric orbit, its irregular and rotating gravity field and the SRP variations due to spacecraft attitude changes. In fact, primitive bodies have generally significant J_2 and orbital eccentricities (≈ 0.2 is common [19]). Because of these strong perturbations it is crucial to transition the ideal orbits found in the previous section to a higher-fidelity model while retaining the advantageous viewing properties. The characteristics of the converged solutions will ultimately dictate if flyable trajectory options exist near the selected RTOs.

Handling irregular gravity field perturbations

This section is focusing on the effect of orbital eccentricity only. In fact, gravity field perturbations can be simply handled by enforcing a minimum radius distance from the body. If the periapsis of the orbit is too low, interactions with the irregular small-body gravity are likely to destabilize the spacecraft motion. According to Scheeres [8], the solar radiation pressure forces are k -times greater than the forces from the small-body shape effects when the following radius constraint is satisfied^{*}:

$$r_p \geq r_{p,k} = \sqrt[4]{k \left(\frac{\mu_{pb}}{\mu_{Sun}} \right)^{2/3} \left(\frac{J_2}{\beta} \right) R^2 r_{pb}^2} \quad (4)$$

where r_{pb} is the average radius of the primitive body. Assuming Bennu data (see Table 2) and $\beta = 30$, we find the effects of SRP and the irregular gravity field forces are of same magnitude when $r_p \geq r_{p,1} = 510 \text{ m} = 0.01 \text{ LU}$. Likewise, the strength of the solar radiation pressure is 10 times larger than the asteroid shape effects when $r_p \geq r_{p,10} = 910 \text{ m} = 0.0175 \text{ LU}$. Orbits with periapsis above $r_{p,1}$ (at least) must be chosen to avoid destabilization effects.

^{*}This result is found by combining Eq. 12, Eq. 75 and Eq. 76 in [8] with our definition of β in Eq. 2

Eccentric Augmented Normalized Hill Three-Body Problem (EANH3BP)

Although the ANH3BP model (described in the background section) has proven fruitful for understanding and selecting RTO orbits, it possesses an inherent approximation, assuming that the small-body orbit is circular. However, the motion of primitive bodies in the solar system is better approximated by elliptic orbits. In particular, this is clearly the case for Bennu with a 0.2 eccentricity. In this section, we therefore introduce a more realistic model by accounting for the eccentricity e of the small-body orbit around the Sun. The Elliptic Augmented Normalized Hill Three-Body Problem (EANH3BP) extends the ANH3BP by assuming that the small body revolves around the distant perturbing body (the Sun) in an elliptic Keplerian orbit rather than a circular one. This new model is therefore more accurate than the ANH3BP and includes time-varying perturbations of the solar pressure and gravity arising from the variation in distance from the Sun. It follows that this model is non-autonomous and does not possess a constant integral of motion (although it is approximately when averaged appropriately [7]). The EANH3BP equation of motion, derived in [7], can be written in the simple following form:

$$\begin{aligned}\ddot{x} &= 2\dot{y} + (1 + e \cos \nu)^{-1} (3x - x/|\mathbf{r}|^3 + \beta) \\ \ddot{y} &= -2\dot{x} + (1 + e \cos \nu)^{-1} (-y/|\mathbf{r}|^3) \\ \ddot{z} &= -z + (1 + e \cos \nu)^{-1} (-z/|\mathbf{r}|^3),\end{aligned}\tag{5}$$

where e is the eccentricity of the elliptic motion of the small body around the Sun, and ν is the true anomaly of the small-body orbit. These equations of motion are given in the same three-body coordinate frame as the ANH3BP (see Eq. 1), but the true anomaly of the small body is used as the independent variable instead of time. This formulation is elegant because the equations contain only two parameters, the eccentricity of the small-body orbit e and the normalized effect of the SRP force β . Note that for $e = 0$ in Eq. 5, we can recover the ANH3BP equations of motion (Eq. 1), i.e. the ANH3BP is a particular case of the EANH3BP. It follows that solutions of the ANH3BP are also solutions of the EANH3BP when the eccentricity vanishes.

Despite being more realistic, the EANH3BP has not been extensively studied in the literature (see [7] for one of the few studies). The remaining of this paper will discuss the main effects of the eccentric perturbation on the ideal RTO orbits and we will use various techniques to transition them in the EANH3BP.

RTO sensitivities to eccentricity

First, in Figure 7, we investigate the behavior of the ideal RTO orbits as the asteroid orbital eccentricity is increased. Note that the states of the ideal RTOs are used directly (at the semilatus rectum in the asteroid orbit, i.e. $\nu = \pi/2$) without any differential correction. Even though the RTOs are linearly stable, we can see that they are fairly sensitive with respect to eccentricity perturbations. Many escaping trajectories are found on the periodic orbit initial conditions from the ANH3BP. In these cases, the perturbations included in the EANH3BP are significant enough to destroy the stable characteristic of these orbits. The RTO families that are destabilized the most by eccentricity are the low-order resonant families. In fact, most of these orbits are too elongated toward the Sun, and the increase in solar radiation pressure at perihelion (induced by the eccentric orbit) can therefore cause escape. It follows that we need a robust approach to find the perturbed RTO orbits in the EANH3BP.

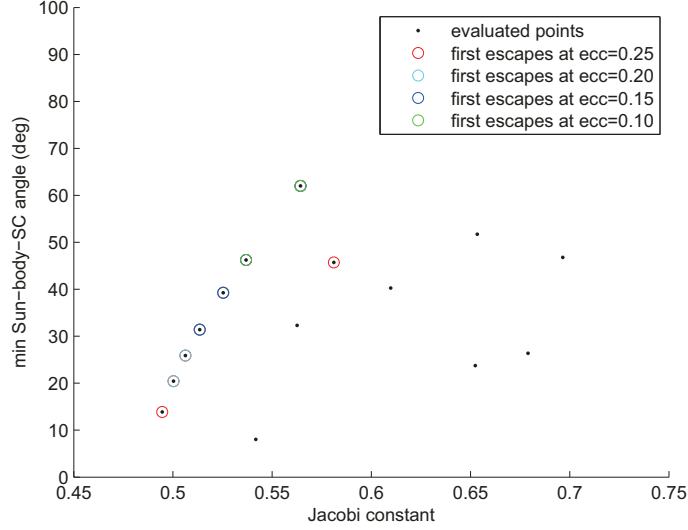


Figure 7: Shows at which eccentricity RTOs at $\beta = 30$ frst escape.

Eccentric RTO tori

The perturbation caused by the small-body orbital eccentricity is periodic with period 2π , as shown in the right hand side of the equations of motion of Eq. 5 (the true anomaly appears only in cosine functions). Consequently, due to this true anomaly dependency, RTO orbits are no longer periodic (unless the period of a RTO orbit is commensurate with 2π). However, since RTO orbits are linearly stable, the eccentric perturbation does not grow after each orbit (to a linear approximation). For small eccentricity at least, it follows that the ideal RTO periodic orbits are replaced with perturbed, quasi-periodic orbits evolving on a 2-D invariant torus parameterized by two incommensurate frequencies: the perturbing frequency $1/(2\pi)$, and a frequency coming from the period of the original periodic orbit of the case $e = 0$.

One way to transition a RTO orbit in the EANH3BP model is therefore to compute explicitly these quasi-periodic invariant tori. A similar idea was successfully implemented for transitioning Halo orbits in the eccentric, restricted three-body problem [16]. In that context, a stroboscopic map $\mathbf{F}_T(\mathbf{X})$ is introduced, where a given initial condition \mathbf{X} is propagated through the flow \mathbf{F} of the EANH3BP for a time T . A fixed point of \mathbf{F}_T corresponds to a T -periodic orbit (for instance, a RTO orbit for $e = 0$). In the same way, a quasi-periodic orbit (with two basic frequencies corresponding to the small body and RTO periods) corresponds to an invariant curve under the map \mathbf{F}_T that can be parameterized by the true anomaly v . The main invariance constraint is:

$$\mathbf{F}_T(\mathbf{X}(v)) - \mathbf{X}(v + \rho) = 0, \quad (6)$$

which must hold for all v . Here T is the period of the RTO orbit and ρ denotes the rotation number of the curve, i.e. the rotation of the states on the curve after winding once around the torus. The rotation number can be expressed with the ratio of the two frequencies of the torus, and is therefore known:

$$\rho = 2\pi \frac{T}{2\pi} = T \quad (7)$$

The invariant curve is computed here by adapting the continuation method developed by Gómez and Mondelo [15] to the eccentric problem, where the invariant curve is discretized over the domain of true anomaly angles and represented via truncated Fourier series. Implementation details of the Gómez and Mondelo procedure can be found in [15].

We applied this method to compute, for increasing eccentricities, quasi-periodic invariant tori of a 8:1 RTO. Unfortunately, tori could be only found for $e < 0.007$, which is far from the 0.2 eccentricity of Benu. The resulting set of quasi-periodic tori are displayed on the Poincare section $\{y = 0, \dot{y} < 0\}$ in Figure 8(b). There are eight fixed points, corresponding to the intersections of the 8:1 RTO periodic orbit. These points are surrounded by elongated curves representing the intersections of the different quasi-periodic tori. In addition, in Figure 8(a), we draw the torus member corresponding maximum eccentricity $e = 0.05$.

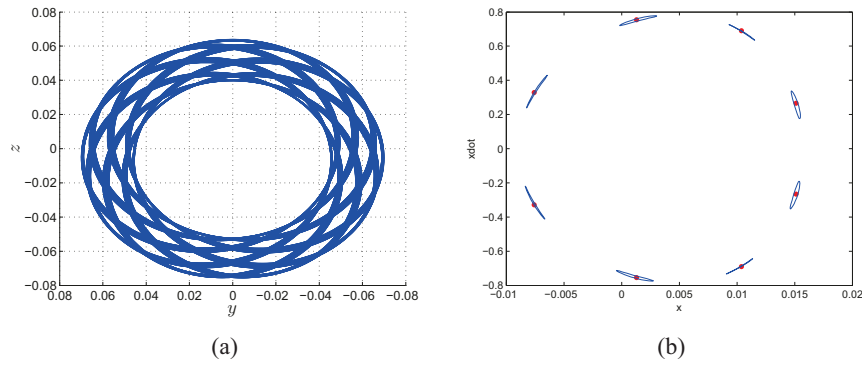


Figure 8: (a) Quasi-periodic torus in EANH3BP for $e = 0.007$. (b) Poincare section of the quasi-periodic torus.

The computed quasi-periodic orbits are confined to a two-dimensional torus as the dynamics of these orbits can be summarized as the composition of two motions: the motion along the periodic RTO orbit and a 2π -periodic motion given by the orbital eccentricity. In reality, there exists a more general quasi-periodic motion evolving on a 3-D torus described by three frequencies, where the third frequency originates from the sun-side unit-magnitude eigenvalue pair of terminator orbits [5] and is incommensurate with the frequency of the orbit. These tori define a 3-D region of phase space and are therefore likely to be more robust to eccentricity perturbations. This full motion was not explored here because the method used in this subsection can only compute 2-D tori described by only two frequencies. It follows that the tori displayed in fig. 8 are a subset of the broader space of quasi-periodic motion near the 6:1 RTO orbit, which may explain why the method was successful for small eccentricities only.

Differential correction and continuation

Differential correction is another method to transition RTO orbits in a higher fidelity model. There exists a wealth of algorithms in the literature. In this section, we propose a multiple-shooting method coupled with a continuation method to smoothly deform a solution from the ANH3BP into the EANH3BP. A similar method was implemented in [20, 21] for obtaining solutions in higher-fidelity models. At each continuation step, the states are computed through the following

parameterization:

$$\mathbf{X}(\lambda) = (1 - \lambda)\mathbf{X}_{\text{ANH3BP}} + \lambda\mathbf{X}_{\text{EANH3BP}} \quad (8)$$

where $0 \leq \lambda \leq 1$, $\mathbf{X}_{\text{ANH3BP}}$ are the states given by the ideal ANH3BP model and $\mathbf{X}_{\text{EANH3BP}}$ are the states of the perturbed EANH3BP model. Starting at $\lambda = 0$, successive multiple shooting sub-problems are solved by slowly increasing the parameter λ and enforcing continuity constraints between the multiple shooting segments. When $\lambda = 1$, the last sub-problem solved corresponds to the desired state values $\mathbf{X}(\lambda = 1) = \mathbf{X}_{\text{EANH3BP}}$. We emphasize that any higher-fidelity model can be considered with this method. In our opinion, this approach is easy to implement and should be quite robust: 1) as opposed to directly switching on the perturbations, a smooth continuation approach is less likely to cause convergence issues; 2) the multiple shooting technique reduces the inherent sensitivity of the problem by splitting the trajectory into multiple segments.

One major challenge of the differential correction method is that it does not preserve the theoretical invariant features and uniqueness of the tori computed in the previous section. In fact, there are no constraints to the end points and therefore the differential corrector problem is not uniquely defined. Instead, in this more practical approach, it is sufficient to converge on a nearby orbit with similar shape and viewing geometries as the original RTO orbit. To enforce greater control over the shape of the trajectory, we therefore apply constraints on the nadir angle and periapsis radius at the intermediate multiple-shooting patch points.

This method is applied to the 6:1 RTO orbit selected in the Osiris-Rex subsection. Unlike the torus method, the orbit can be transitioned to the EANH3BP with a 0.2 eccentricity. The resulting orbit, propagated for six months, is depicted in Figure 9 along with its groundtrack relative to the Sun. Evolution of minimum nadir pointing phase angle, minimum periapsis radius and maximum apoaapsis radius are given in Figure 10 and Figure 11. We can see that the geometry of the converged orbit is similar to that of the original RTO orbit, apart from long-term sinusoidal variations associated with the orbital eccentricity. The geometry constraints defined in the Osiris-Rex subsection are all met (min $\phi < 50$ deg, min radius < 510 m, max radius ≈ 5 km). As hypothesized in the previous subsection, the geometry of the Poincare section crossings in Figure 10(a) suggests that the trajectory is near a 3-D quasi-periodic torus.

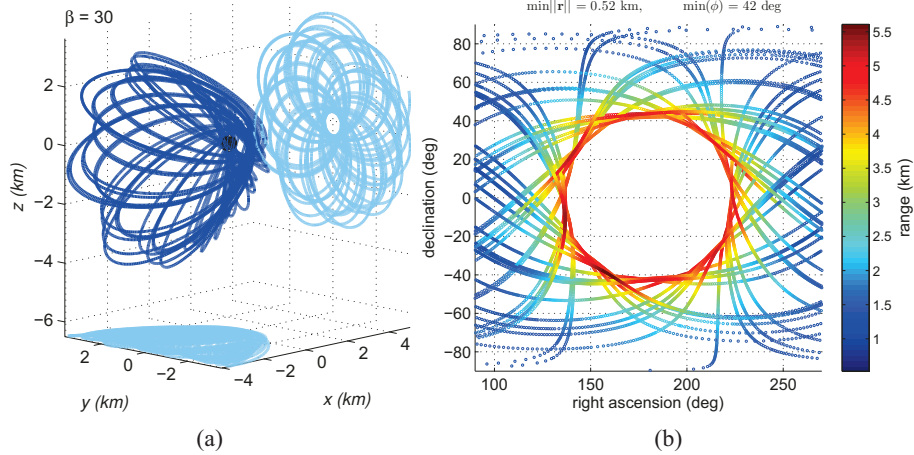


Figure 9: Spatial plot (a) and groundtrack/altitude relative to the Sun (b) for converged example mapping trajectory consistent with the upcoming OSIRIS-REx mission.

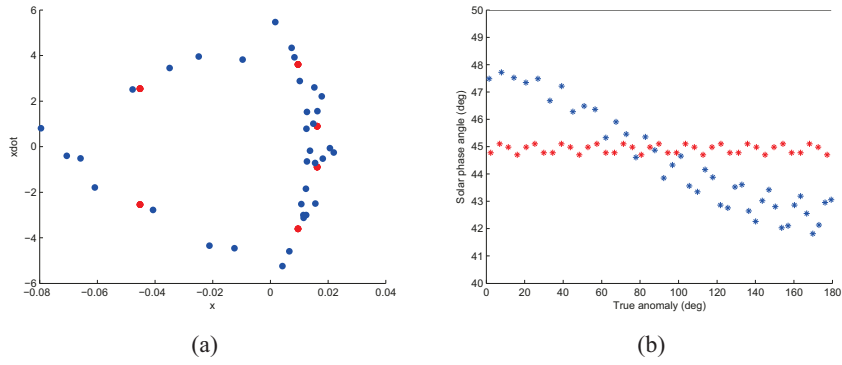


Figure 10: (a) Ideal RTO orbit (red) versus transitioned RTO orbit (blue) on a Poincaré section. (b) Evolution of minimum nadir pointing phase angle.

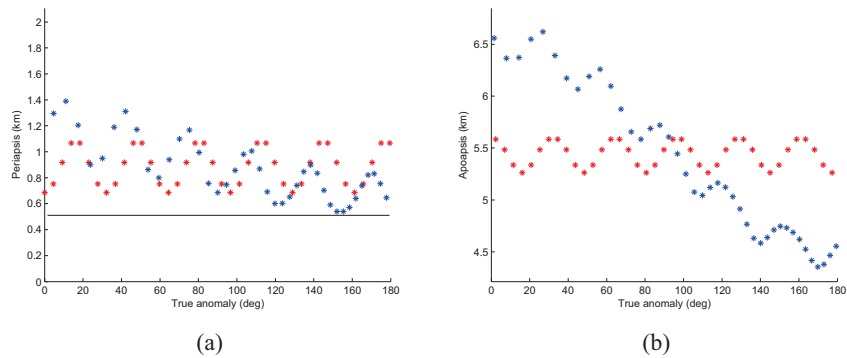


Figure 11: Evolution of apsides for the ideal (red) and differentially-corrected (blue) RTO orbit. (a) Minimum periapsis radius. (b) Maximum apoapsis radius.

CONCLUSION

A simple design methodology was introduced to select a quasi-terminator orbit suitable for the global mapping requirements of a given mission. It was found that there are two degrees of freedom for the selection of the orbital parameters, including minimum nadir pointing phase angle and minimum periapsis. In addition, the effect of the eccentricity of the small-body orbit on these orbits was investigated. In particular, several algorithms are suggested to transition these orbits in this higher-fidelity model. The transitioned orbits are shown to retain good geometry characteristics, although they are no longer periodic. An example of appropriate quasi-terminator orbit for the upcoming OSIRIS-REx mission has been selected and transitioned in the higher-fidelity eccentric model, which demonstrates the applicability of quasi-terminator orbits to this mission.

In future work, the complex gravity field of the primitive body will be added in the differential correction process. We will also investigate the computation of 3-D sun-side QTO tori in the eccentric problem. Finally, a better understanding of the design space is required for the timely design of observation cadences and other high-level constraints.

ACKNOWLEDGEMENTS

The work described in this paper was carried out at the Jet Propulsion Laboratory, California Institute of Technology, under a contract with the National Aeronautics and Space Administration. The authors thank Zubin Olikara for helpful discussions on the computation of quasi-periodic tori in eccentric three-body models.

REFERENCES

- [1] S. B. Broschart and D. J. Scheeres. Control of hovering spacecraft near small-bodies: Application to asteroid 25143 itokawa. *Journal of Guidance, Control, and Dynamics*, 28(2):343–354, 2005.
- [2] Personal correspondance with Dr. Dan Scheeres, 2013.
- [3] P. Michel, M. A. Barucci, A. F. Cheng, H. Bhnhardt, J. R. Brucato, E. Dotto, P. Ehrenfreund, I. A. Franchi, S. F. Green, L. M. Lara, B. Marty, D. Koschny, and D. Agnolon. Marcopolo-r: Near-earth asteroid sample return mission selected for the assessment study phase of the esa program cosmic vision. *Acta Astronautica*, 2012.
- [4] D. J. Scheeres. Orbit mechanics about small asteroids. *Advances in the Astronautical Sciences*, 134:1795–1812, 2009. AAS Paper 09-220.
- [5] S.B. Broschart, G. Lantoine, and D. J. Grebow. Characteristics of quasi-terminator orbits near primitive bodies. presented at the 2013 AAS/AIAA Spaceflight Mechanics Meeting, February 2013, Kauai, Hawaii, AAS 13-335.
- [6] Stephen B. Broschart, Gregory Lantoine, and Daniel J. Grebow. Quasi-terminator orbits near primitive bodies. *Celestial Mechanics and Dynamical Astronomy manuscript*, 2013.
- [7] D. J. Scheeres and F. Marzari. Spacecraft dynamics in the vicinity of a comet. *Journal of the Astronautical Sciences*, 50(1):35–52, 2002.
- [8] D. J. Scheeres. Satellite dynamics about asteroids. *Advances in the Astronautical Sciences*, 87:275–292, 1994. AAS Paper 94-112.
- [9] Harry Dankowicz. Some special orbits in the two-body problem with radiation pressure. *Celestial Mechanics and Dynamical Astronomy*, 58:353–370, 1994.
- [10] Daniel J. Scheeres. Satellite dynamics about small bodies: Averaged solar radiation pressure effects. *Journal of the Astronautical Sciences*, 47(1):25–46, 1999.
- [11] S. B. Broschart and B. F. Villac. Identification of non-chaotic terminator orbits near 6489 golevka. *Advances in the Astronautical Sciences*, 134:861–880, 2009. AAS Paper 09-156.
- [12] Stephen B. Broschart, Daniel J. Scheeres, and Benjamin F. Villac. New families of multi-revolution terminator orbits near small bodies. *Advances in the Astronautical Sciences*, 135:1685–1702, 2010. AAS Paper 09-402.
- [13] (Katherine) Yi-Yin Liu and Benjamin Villac. Periodic orbit families in the hill’s three-body problem with solar radiation pressure. *Advances in the Astronautical Sciences*, 136:285–300, 2010. AAS Paper 10-118.
- [14] K.C. Howell and J.V. Breakwell. Almost rectilinear halo orbits. *Celestial Mechanics*, 32(6):29–52, 1984.
- [15] Gerard Gómez and Josep M. Mondelo. The dynamics around the collinear equilibrium points of the rtbp. *Physica*, 154(4):283–321, 2001.
- [16] Zubin P. Olikara and Daniel J. Scheeres. Numerical methods for computing quasi-periodic orbits and their stability in the restricted three-body problem. presented at the 1st IAA Conference on Dynamics and Control of Space Systems, 2010, Paper 08-10, 2010.
- [17] E. Kolemen, N. Kasdin, and P. Gurf1. Multiple poincar sections method for fnding the quasisperiodic orbits of the restricted three body problem. *Celestial Mechanics and Dynamical Astronomy*, 112(1):47–74, 2012.
- [18] Personal communication with Kevin Berry, GSFC, 2013.
- [19] JPL’s Horizons System. Website, December 2003. <http://ssd.jpl.nasa.gov/horizons.html>.
- [20] R. P. Russell and N. J. Strange. Planetary moon cyler trajectories. *Journal of Guidance, Control, and Dynamics*, 32(1):143–157, 2009.
- [21] G. Lantoine and R. P. Russell. Near-ballistic halo-to-halo transfers between planetary moons. *Journal of the Astronautical Sciences*, 58(3):335–363, 2011.